Mon. Not. R. Astron. Soc. **000**, 000–000 (0000) Printed October 5, 2012 (MN LATEX style file v2.2)

The runaway instability in general-relativistic accretion disks

O. Korobkin[1,2⋆], E. Abdikamalov[3]†, N. Stergioulas[4], E. Schnetter[5,6,7], B. Zink[8], S. Rosswog[2], and C. D. Ott[3]

[1]*School of Engineering and Science, Jacobs University Bremen, Germany*
[2]*Astronomy and Oskar Klein Centre, Stockholm University, Sweden*
[3]*TAPIR, California Institute of Technology, USA*
[4]*Department of Physics, Aristotle University of Thessaloniki, Greece*
[5]*Perimeter Institute for Theoretical Physics, Canada*
[6]*Department of Physics, University of Guelph, Canada*
[7]*Center for Computation & Technology, Louisiana State University, USA*
[8]*Theoretical Astrophysics, University of Tübingen, Germany*

October 5, 2012

ABSTRACT

When an accretion disk falls prey to the runaway instability, a large portion of its mass is devoured by the black hole within a few dynamical times. Despite decades of effort, it is still unclear under what conditions such an instability can occur. The technically most advanced relativistic simulations to date were unable to find a clear sign for the onset of the instability. In this work, we present three-dimensional relativistic hydrodynamics simulations of accretion disks around black holes in dynamical spacetime. We focus on the configurations that are expected to be particularly prone to the development of this instability. We demonstrate, for the first time, that the fully self-consistent general relativistic evolution does indeed produce a runaway instability.

Key words: accretion disks, runaway instability, gamma-ray bursts, numerical relativity

1 INTRODUCTION

Thick and massive relativistic accretion disks around black holes (BHs) are thought to form in extreme core-collapse events of massive stars (Woosley 1993; MacFadyen & Woosley 1999; Sekiguchi & Shibata 2011; Ott et al. 2011; Woosley & Heger 2012), and they are a normal outcome for the coalescense of neutron star (NS)-NS (e.g., Ruffert et al. 1997; Rosswog et al. 2003; Shibata & Taniguchi 2006; Oechslin & Janka 2006; Baiotti et al. 2008; Liu et al. 2008; Kiuchi et al. 2009) and NS-BH binaries (e.g., Rosswog 2005; Shibata & Uryū 2006; Shibata et al. 2009; Etienne et al. 2009; Chawla et al. 2010; Ruffert & Janka 2010; Foucart et al. 2011). Such systems are thought to be candidates for the central engines of gamma-ray bursts (GRBs, Popham et al. 1999; Woosley 1993; Piran 2004; Lee & Ramirez-Ruiz 2007; Mészáros & Gehrels 2012).

Previous studies of the stability of accretion disks have shown that they can be subject to various types of global instabilities in a number of scenarios (e.g., Abramowicz et al. 1983; Papaloizou & Pringle 1984, 1985; Kojima 1986; Woodward et al. 1994; Font & Daigne 2002b; Zanotti et al. 2003; Taylor et al. 2011; Korobkin et al. 2011; Kiuchi et al. 2011). Instabilities can result in strongly variable and unstable accretion rates. Abramowicz et al. (1983) discovered the so-called dynamical runaway instability (RI) in thick, self-gravitating accretion disks around BHs. The RI is similar to the dynamical instability in close binary systems that occurs when the more massive binary member overflows its Roche lobe. In this case, the size of the Roche lobe decreases faster than the size of the binary companion, which can ultimately lead to the tidal disruption of the companion and the merger of the binary system. In disks around BHs, a toroidal surface analogous to the Roche lobe can be identified. A meridional cut of this surface exhibits a cusp located at the L_1 Lagrange point. If the disk overflows this toroidal Roche surface, then the mass-transfer through the cusp will push the cusp outwards, making a larger fraction of the disk matter unstable to accretion. This drives the cusp out even further, and leads to an exponential growth of the mass-transfer rate. As a result, most of the disk gets consumed by the BH within just a few dynamical times.

Abramowicz et al. (1983) found that the development

⋆ E-mail: oleg.korobkin@astro.su.se
† E-mail: abdik@tapir.caltech.edu

of the RI depends on a wide range of parameters, such as the disk-to-BH mass ratio $M_{\rm D}/M_{\rm BH}$ and the location of the inner edge of the disk[1]. However, their investigation was based on several approximations and simplifications: they used a polytropic equation of state (EOS) for the disk material, a pseudo-Newtonian potential to model gravity of BH (Paczynsky & Wiita 1980), a disk with constant specific angular momentum, and an approximate treatment of the self-gravity of the disk. Subsequent works with more refined approximations found indications of a stabilizing effect due to BH rotation (Wilson 1984; Abramowicz et al. 1998), while a positive radial gradient of specific angular momentum was suggested to strongly suppress the instability (Abramowicz et al. 1998; Daigne & Mochkovitch 1997; Font & Daigne 2002a; Daigne & Font 2004). Moreover, studies using a Newtonian pseudopotential for the gravity of the BH (Khanna & Chakrabarti 1992; Masuda et al. 1998) and relativistic calculations in a fixed spacetime background (Nishida et al. 1996; Font & Daigne 2002b) found that the self-gravity of the disk aggravates the instability. Nevertheless, the distance between the inner edge of the disk and the location of the cusp is probably the most crucial parameter for the development of the RI: for as long as it is too large, the RI is unlikely to occur.

Recently, Montero et al. (2010) performed the first fully general relativistic simulations of thick accretion disks around BHs in axisymmetry for a few dynamical times. For the particular models they studied, they found no signature of a RI during the simulated time. However, the inner surface of their disk models was located away from the Roche surfaces (P. Montero, private communication), so that the instability might not have had sufficiently favourable conditions or sufficient time to develop within the time period of disk evolution that was considered. Therefore, their results do not rule out the existence of the RI in disk models where the inner edge is located closer to the cusp.

In Korobkin et al. (2011), some of us have analyzed the stability of slender and moderately slender accretion disks around BHs with $M_{\rm D}/M_{\rm BH}$ in the range of (0.11, 0.24) using three-dimensional (3D) numerical simulations in full general relativity (GR). Although we did observe the development of several non-axisymmetric instabilities in our models, we found no traces of the RI. This result is, perhaps, not surprising since the inner radii of our disk models were located significantly away from the Roche surface (see Korobkin et al. (2011) for more details).

In a similar study, Kiuchi et al. (2011) performed simulations of self-gravitating disks around BHs in full GR with the aim of obtaining the gravitational wave signal from the non-axisymmetric Papaloizou-Pringle instability. They considered four disk models with constant and non-constant specific angular momentum and disk-to-BH mass ratios of 0.06 and 0.10. No runaway instability was observed in their simulations, but no information was given regarding the relative location of the inner edge of the disk and the Roche surface. Therefore, it is difficult to judge if their models were sufficiently susceptible to develop the RI.

In order to understand whether the RI can occur at all in the most general case, one first has to expore whether it can develop in configurations that are *particularly prone* to the instability. Such systems contain disks that exactly fill their Roche lobes, have significant fractions of the BH masses, constant specific angular momentum profiles and non-rotating BHs[2]. It is left to future studies to explore under which circumstances such configurations would form in Nature. Our aim here is to explore whether the RI can occur *in principle* if the fully dynamical general-relativistic effects are taken into account properly. Our 3D general relativistic simulations indeed confirm that the RI occurs in these cases.

This paper is organized as follows. In Section 2, we describe the numerical methods used in our simulations. In Section 3, we describe the initial disk model. In Section 4, we present our results, and in Section 5 present our conclusions for future work. Unless otherwise noted, throughout the paper we measure distances in the units of the Schwarzschild radius $r_g = 2GM_{\rm BH}(0)/c^2$ of the black hole at $t = 0$, while the rest of the quantities are measured in cgs units.

2 NUMERICAL METHODS

The numerical time-evolution in our study is performed with the GR hydrodynamics code THOR (Zink et al. 2008) and the spacetime evolution code QUILT (Pazos et al. 2007). These two codes are based on and communicate with each other via the open-source CACTUS computational infrastructure (Goodale et al. 2003; Schnetter et al. 2007), and use the CARPET mesh refinement and multiblock driver (Schnetter et al. 2004; Schnetter et al. 2006). Initial models of self-gravitating disks around BHs are constructed using an improved version of the RNS code (Stergioulas 2011). We use a multiblock grid with an adapted resolution which is similar to the one used in Korobkin et al. (2011). The grid resolution is $\Delta_{\rm min} \sim 0.022\, r_g$ near the BH, $\Delta_{\rm max} \sim 0.2\, r_g$ at the disk density maximum, and $\Delta_{\rm out} \sim 5.0\, r_g$ at the outer boundary. For more details of the numerical methods as well as the grid structure used in our simulations, we refer the reader to Korobkin et al. (2011).

3 INITIAL DISK MODEL

In this study, we focus on two initial disk models, denoted A and B. Table 1 lists the parameters of these models, while Fig. 1 illustrates the structure of initial model A. We construct our disks using a polytropic EOS $p = K\rho^\Gamma$ with $\Gamma = 4/3$, while the time-evolution is performed with the two-parameter ideal gas EOS (with the same Γ), which allows for shock heating. We do not include additional physics such as magnetic fields, nuclear or neutrino processes. Therefore, the results can be rescaled using one free parameter such as the initial BH mass. In particular, the cgs parameters listed

[1] Here, the term "disk" refers to initial equilibrium disk configurations. Therefore, the concept of the inner edge for such systems is well defined. Note, however, that disk tend to spread on a viscous timescale.

[2] BH+disk systems with slowly rotating BHs are unlikely to be drastically different from non-rotating BH cases. Nevertheless, the latter are expected to be more susceptible to the RI, that is why they are in the focus of our work.

Model	A	B
Specific angular momentum ℓ $[M_{BH}]$	3.91	3.84
Polytropic constant K $[10^{14}\mathrm{cm}^3\mathrm{g}^{-1/3}\mathrm{s}^{-2}]$	5.35	5.72
Maximum density $\rho_{\max}$ $[10^{12}\mathrm{g/cm}^3]$	1.63	1.33
Disk-to-BH mass ratio M_D/M_{BH}	0.2097	0.1628
Kinetic to potential energy $T/\lvert U\rvert$	0.2666	0.2469
Inner radius $r_{\rm in}[r_g]$	2.082	2.127
Location of the cusp $r_L[r_g]$	2.024	2.148
Outer radius $r_{\rm out}[r_g]$	12.08	12.37
Central radius $r_{\max}[r_g]$	4.687	4.342
Orbital frequency at $r_{\max}$, $\Omega_{\max}$ $[\mathrm{s}^{-1}]$	1414	1581
Orbital period at $r_{\max}$, $P_{\max}$ [s]	$4.44\cdot10^{-3}$	$3.96\cdot10^{-3}$
Potential gap $\Delta W := W_{\rm in} - W_L$	$-1.2\cdot10^{-4}$	$+0.01$

Table 1. Physical parameters of the initial disk models used. Notice that the specific angular momentum and ΔW are given in units of $c = G = 1$.

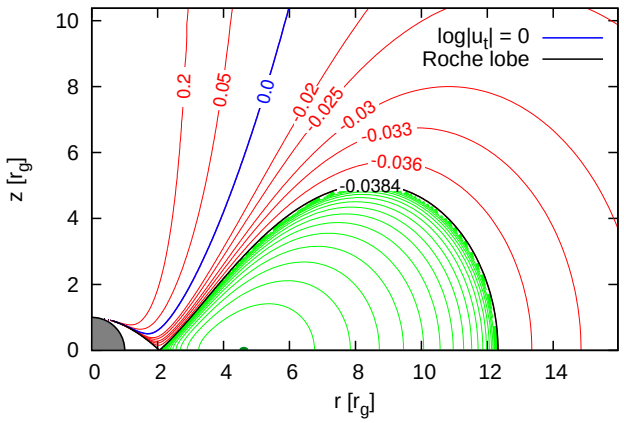

Figure 1. The structure of the initial disk model A. Red and green lines show the contours of the effective potential $W = \log|u_t|$ and of the disk pressure, respectively. Here, u_t is the covariant t-component of the 4-velocity of a test particle on a circular orbit with the given specific angular momentum for model A. The values of W are given in geometrized units $G = c = 1$. Contours of the pressure are equally spaced by 0.5 in decimal logarithmic scale, starting from the maximum pressure (green dot on the r-axis). The blue contour corresponds to $W = 0$, and the black contour marks the location of the toroidal Roche lobe with the cusp. The disk fills the Roche lobe almost up to the cusp. The gray area marks the location of the BH event horizon.

in Table 1 assume $\mathcal{M}_{\rm BH} = 5\ \mathcal{M}_\odot$. The disk-to-BH mass ratio $\mathcal{M}_{\rm disk}/\mathcal{M}_{\rm BH}$ is ≈ 0.21 for model A and ≈ 0.16 for model B. Both disks have a constant specific angular momentum profile. The black contour in Fig. 1 corresponds to the Roche surface, while the green ones show the contours of constant pressure. The disk in model A fills its Roche lobe almost entirely, with a remaining gap in the effective potential between the inner edge of the disk and the cusp of only $\Delta W = -1.2\times10^{-4}$. By contrast, model B is constructed to slightly overfill its Roche lobe by the value $\Delta W = 0.01$. This is done in order to induce the onset of the RI right from the very beginning of the numerical evolution.

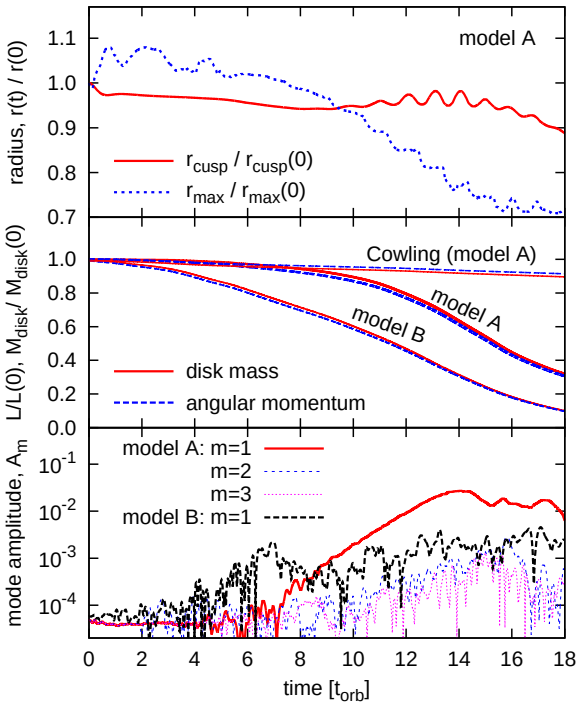

Figure 2. Evolution of the disk. *Top*: radial location of the cusp and the disk density maximum, normalized to their initial values. *Centre*: evolution of the disk rest mass and angular momentum for models A and B in full GR as well as for model A in the Cowling approximation. For clarity, the deviations from 1 of the mass and angular momentum in Cowling are multiplied by a factor of 10. *Bottom*: Normalized amplitudes of non-axisymmetric $m = 1, 2, 3$ deformations in model A and $m = 1$ deformation in model B.

4 RESULTS

Models A and B both develop the runaway instability. Therefore, in the following, we concentrate on the results for model A, while model B will be discussed later in this section. The top panel of Fig. 2 shows the time evolution of the cusp radius and the radial coordinate of the location of the maximum disk density $r_{\max}$. Due to initial metric perturbations induced by matching the initial data to a vacuum BH metric near the horizon (cf. discussion in Korobkin et al. 2011), the BH mass and cusp radius settle to a new, $\sim 3\%$ smaller value within $t \lesssim 0.5t_{\rm orb}$. The smaller gravitational pull of the BH leads to a rapid increase of $r_{\max}$ by $\sim 9\%$ within the same time interval. Since the cusp is now located at a smaller radius, the disk is less likely to become subject to the RI. However, the initial metric perturbations induce oscillations in the disk, which are particularly evident in the evolution of $r_{\max}$ at $t \lesssim 6t_{\rm orb}$. These oscillations lead to occasional crossing of the Roche lobe by the disk, resulting in a steady and slow accretion of the disk material onto the BH at $t \lesssim 9t_{\rm orb}$. This is visible in the evolution of the disk mass and angular momentum shown in the center panel of Fig. 2.

The radius $r_{\max}$ gradually decreases due to this slow accretion up to the time when the inner disk radius becomes as small as the cusp radius. This occurs at $t \sim 9t_{\rm orb}$. At that point, the cusp radius starts increasing, leading to an

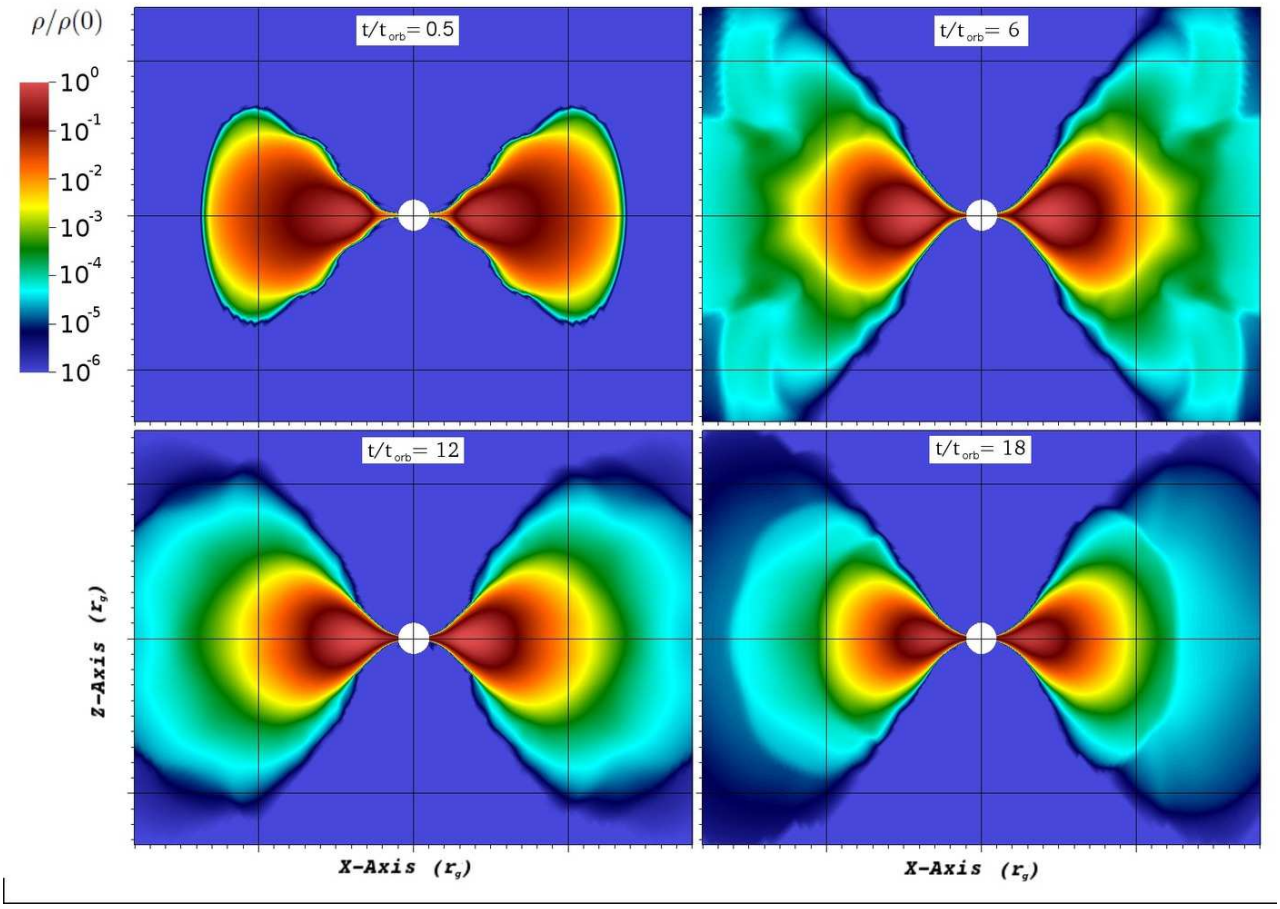

Figure 3. Colourmaps of the disk density in the vertical plane at different times in evolution of model A. Here, $t_{\rm orb}$ is the orbital period at the maximum density radius $r_{\rm max}$.

acceleration of the accretion. By the end of our simulation ($t = 18t_{\rm orb}$), $\sim 75\%$ of the initial disk mass has been accreted onto the BH. Such an accelerated accretion due to dynamical migration of the cusp towards the disk during which most of the disk material is swallowed by the BH is exactly the defining property of the runaway instability. Thus, our simulations show that the RI can indeed occur, at least for the most susceptible models, which are considered here.

It is interesting to note that the development of the axisymmetric runaway instability triggers non-axisymmetric deformations of the disk. The bottom panel of Fig. 2 shows the normalized amplitude of non-axisymmetric $m = 1, 2, 3$ deformations (see Korobkin et al. (2011) for the exact definition of the amplitude). The $m = 1$ deformation grows exponentially starting at $\sim 7t_{\rm orb}$ until $\sim 14t_{\rm orb}$, reaches its peak value of ~ 0.027, at which point it saturates. This deformation develops due to the so-called Papaloizou and Pringle instability (PPI) (Papaloizou & Pringle 1984), enhanced by an eccentric motion of the BH (as described in Korobkin et al. 2011). The deformations corresponding to the other values of m do not show a strong growth and remain below $\sim 10^{-3}$. Since both the PPI and RI develop roughly at the same time in our simulations, they could, in principle, interact non-linearly, when sufficiently large amplitudes are reached. In particular, the PPI-induced deformations might be responsible for the apparent saturation of the RI towards the end of our simulations. Such deformations redistribute angular momentum outwards, which, in turn, inhibits the development of the RI (Daigne & Font 2004) (while another factor responsible for the eventual saturation of the RI is, of course, the depletion of the disk mass). Nevertheless, the rather moderate amplitude of the $m = 1$ mode of ~ 0.027 is unlikely to drastically affect the evolution of the RI, especially during the early evolution. A more detailed analysis of the non-linear interaction between the PPI and the RI is required to clarify its role.

Figure 3 shows four snapshots of the disk density in the meridional plane, for model A, corresponding to the times $t/t_{\rm orb} = 0.5$, 6, 12 and 18. The snapshot at $t = 0.5\ t_{\rm orb}$ shows the disk in a perturbed state after the passage of the initial metric perturbation. As the disk moves away from the BH, several surface waves can be seen propagating to the outer side of the disk in an axisymmetric manner. As noted above, such waves have sufficiently high amplitude to overfill the Roche lobe and support a small amount of accretion. The next snapshot at $t = 6\ t_{\rm orb}$ shows a wider accretion stream and an extended structure of the outer parts of the disk, caused by heating by the shocks formed during the radial disk oscillations. Such shock heating efficiently damps out the radial disk oscillation and causes the disk to heat up and expand, similarly to what was observed in Korobkin et al.

(2011). The last two snapshots show the disk during the rapid accretion phase at $t = 12\ t_{\rm orb}$ and $t = 18\ t_{\rm orb}$. By $t = 18\ t_{\rm orb}$, the accretion stream is very wide, but the high-density parts have moved closer to the black hole and occupy a smaller volume, indicating a smaller disk mass.

To secure our findings against the possibility of an error in the treatment of hydrodynamics, we have complemented the fully dynamical GR simulation of model A with one in the Cowling approximation (i.e., on a fixed metric background). Such a model should undergo at most a slow and steady accretion, in a way similar to the early ($t \lesssim 6t_{\rm orb}$) evolution of the fully dynamical model. There should be no unstable growth of accretion on a fixed metric background. As we can see from the time evolution of the disk mass and angular momentum shown in the center panel of Fig. 2, this is indeed the case.

Interestingly, model A does not develop the PPI in our Cowling simulation, where amplitudes of non-axisymmetric deformations remain below $\sim 10^{-5}$ throughout the evolution. Since the PPI in Cowling approximation relies on the existence of the non-accreting inner edge of the disk (Blaes 1987; Hawley 1991), the absence of PPI is probably caused by the accretion at a small rate through the cusp, which can completely freeze the development of PPI modes in Cowling approximation (Blaes 1987; Hawley 1991). This is different in the case of a dynamical metric, where the PPI can be enhanced by the motion of the BH (Korobkin et al. 2011). For this reason, accretion fails to suppress the PPI in model A with a dynamical metric (this is also observed in Fig. 1 of Kiuchi et al. (2011) for the models with constant specific angular momentum).

Compared to model A, in model B the disk overflows its Roche lobe by a small amount $\Delta W = 0.01$. In this case, the exponential accretion should commence immediately and continue until a significant fraction of the disk is accreted onto the BH within a few dynamical times. This is what we observe in our simulation, as can be seen from the evolution of the disk mass and angular momentum shown in the center panel of Fig. 2. Notice, however, that in this case the development of the instability happens more slowly, because of the lower disk-to-BH mass ratio. The amplitude of non-axisymmetric deformations is also lower. In particular, the $m = 1$ mode exhibits slow and irregular growth and stays below $\sim 10^{-3}$ throughout the simulation (cf. the center panel of Fig. 2). In the absence of any significant non-axisymmetic deformation, the accretion of a substantial fraction of the disk mass onto the BH within a few dynamical times can only be attributed to the development of the RI.

As mentioned in Section 1, Montero et al. (2010) presented axisymmetric simulations of two disk models around BHs with a constant specific angular momentum. Their simulations were also fully general relativistic with dynamical spacetime evolution, similar to our simulations. The absence of the RI in Montero et al. (2010) must be attributed to differences in the initial disk models (compared to our configurations) and specifically to the fact that their initial models did not exactly fill the Roche lobe. Because of this, the instability is less likely to occur within the limited simulation time. The same argument may explain the absence of the RI in Kiuchi et al. (2011). If confirmed, this would further underline the importance of the distance between the cusp and the inner disk surface for the development of RI.

5 CONCLUSION

In this study, we have, for the first time, demonstrated that the runaway instability in self-gravitating accretion disks does indeed occur in fully dynamical general relativistic evolutions. We have selected two models that are particularly prone to the development of such an instability. Our models have an appreciable disk-to-BH mass ratio (0.21 for model A and 0.16 for model B, see Table 1), a constant profile of specific angular momentum and a non-rotating BH. Moreover, and perhaps most importantly for the development of the runaway instability, our disk model A almost exactly fills its Roche lobe, while model B slightly overfills it.

Our simulations show that both models develop the runaway instability, exhibiting unstable accretion of the disk matter onto the BH within just a few dynamical times. More than half of the disk mass is absorbed by the BH by the end of our simulations, which were terminated only because we ran out of available computing time.

Our results demonstrate that the runaway instability does indeed occur, at least in the models considered here. Future research will need to investigate how this depends on the parameters of the initial disk models, such as the disk-to-BH mass ratio, the gradient of the specific angular momentum of the disk, and the BH spin, in order to establish the astrophysical significance of the instability.

6 ACKNOWLEDGEMENTS

We acknowledge stimulating discussions with P. Diener, P. Montero, C. Reisswig, M. Scheel, B. Szilágyi, and J. Tohline. This work is supported by the National Science Foundation under grant numbers AST-1212170, PHY-1151197, PHY-1212460, and OCI-0905046, by the German Research Foundation grant DFG RO-3399, AOBJ-584282, and by the Sherman Fairchild and Alfred P. Sloan Foundation. NS acknowledges support by an Excellence Grant of the research committee of the Aristotle University of Thessaloniki. Supercomputing simulations for this article were performed on the Compute Canada SHARCNET cluster "Orca" (project CFZ-411-AA), Caltech compute cluster "Zwicky" (NSF MRI award No. PHY-0960291), on the NSF XSEDE network under grant TG-PHY100033, on machines of the Louisiana Optical Network Initiative under grant loni_numrel07, and at the National Energy Research Scientific Computing Center (NERSC), which is supported by the Office of Science of the US Department of Energy under contract DE-AC03-76SF00098.

References

Abramowicz M. A., Calvani M., Nobili L., 1983, Nature, 302, 597

Abramowicz M. A., Karas V., Lanza A., 1998, A&A, 331, 1143

Baiotti L., Giacomazzo B., Rezzolla L., 2008, Phys. Rev. D, 78, 084033

Blaes O. M., 1987, MNRAS, 227, 975

Chawla S., Anderson M., Besselman M., Lehner L., Liebling S. L., Motl P. M., Neilsen D., 2010, Phys. Rev. Lett., 105, 111101

Daigne F., Font J. A., 2004, MNRAS, 349, 841

Daigne F., Mochkovitch R., 1997, MNRAS, 285, L15
Etienne Z. B., Liu Y. T., Shapiro S. L., Baumgarte T. W., 2009, Phys. Rev. D, 79, 044024
Font J. A., Daigne F., 2002a, ApJ, 581, L23
Font J. A., Daigne F., 2002b, MNRAS, 334, 383
Foucart F., Duez M. D., Kidder L. E., Teukolsky S. A., 2011, Phys. Rev. D, 83, 024005
Goodale T., Allen G., Lanfermann G., Massó J., Radke T., Seidel E., Shalf J., 2003, in Vector and Parallel Processing – VECPAR'2002, 5th International Conference, Lecture Notes in Computer Science The Cactus framework and toolkit: Design and applications. Springer, Berlin
Hawley J. F., 1991, ApJ, 381, 496
Khanna R., Chakrabarti S. K., 1992, MNRAS, 259, 1
Kiuchi K., Sekiguchi Y., Shibata M., Taniguchi K., 2009, Phys. Rev. D, 80, 064037
Kiuchi K., Shibata M., Montero P. J., Font J. A., 2011, Phys. Rev. Lett., 106, 251102
Kojima Y., 1986, Prog. Theor. Phys., 75, 251
Korobkin O., Abdikamalov E. B., Schnetter E., Stergioulas N., Zink B., 2011, Phys. Rev. D, 83, 043007
Lee W. H., Ramirez-Ruiz E., 2007, New Jour. Phys., 9, 17
Liu Y. T., Shapiro S. L., Etienne Z. B., Taniguchi K., 2008, Phys. Rev. D, 78, 024012
MacFadyen A. I., Woosley S. E., 1999, ApJ, 524, 262
Masuda N., Nishida S., Eriguchi Y., 1998, MNRAS, 297, 1139
Mészáros P., Gehrels N., 2012, Research in Astronomy and Astrophysics, 12, 1139
Montero P. J., Font J. A., Shibata M., 2010, Phys. Rev. Lett., 104, 191101
Nishida S., Lanza A., Eriguchi Y., Abramowicz M. A., 1996, MNRAS, 278, L41
Oechslin R., Janka H., 2006, MNRAS, 368, 1489
Ott C. D., Reisswig C., Schnetter E., O'Connor E., Sperhake U., Löffler F., Diener P., Abdikamalov E., Hawke I., Burrows A., 2011, Phys. Rev. Lett., 106, 161103
Paczynsky B., Wiita P. J., 1980, Astron. Astrophys., 88, 23
Papaloizou J. C. B., Pringle J. E., 1984, MNRAS, 208, 721
Papaloizou J. C. B., Pringle J. E., 1985, MNRAS, 213, 799
Pazos E., Dorband E. N., Nagar A., Palenzuela C., Schnetter E., Tiglio M., 2007, Class. Quantum Grav., 24, 341
Piran T., 2004, Rev. Mod. Phys., 76, 1143
Popham R., Woosley S. E., Fryer C., 1999, ApJ, 518, 356
Rosswog S., 2005, ApJ, 634, 1202
Rosswog S., Ramirez-Ruiz E., Davies M. B., 2003, MNRAS, 345, 1077
Ruffert M., Janka H., 2010, A&A, 514, A66+
Ruffert M., Rampp M., Janka H., 1997, A&A, 321, 991
Schnetter E., Diener P., Dorband E. N., Tiglio M., 2006, Class. Quantum Grav., 23, S553
Schnetter E., Hawley S. H., Hawke I., 2004, Class. Quantum Grav., 21, 1465
Schnetter E., Ott C., Allen G., Diener P., Goodale T., Radke T., Seidel E., Shalf J., 2007, CoRR, abs/0707.1607
Sekiguchi Y., Shibata M., 2011, ApJ, 737, 6
Shibata M., Kyutoku K., Yamamoto T., Taniguchi K., 2009, Phys. Rev. D, 79, 044030
Shibata M., Taniguchi K., 2006, Phys. Rev. D, 73, 064027
Shibata M., Uryū K., 2006, Phys. Rev. D, 74, 121503
Stergioulas N., 2011, Int. J. Mod. Phys. D, 20, 1251
Taylor P. A., Miller J. C., Podsiadlowski P., 2011, MNRAS, 410, 2385
Wilson D. B., 1984, Nature, 312, 620
Woodward J. W., Tohline J. E., Hachisu I., 1994, ApJ, 420, 247
Woosley S. E., 1993, ApJ, 405, 273
Woosley S. E., Heger A., 2012, ApJ, 752, 32
Zanotti O., Rezzolla L., Font J. A., 2003, MNRAS, 341, 832
Zink B., Schnetter E., Tiglio M., 2008, Phys. Rev. D, 77, 103015

This paper has been typeset from a TEX/ LATEX file prepared by the author.

This figure "figure3.png" is available in "png" format from:

http://arxiv.org/ps/1210.1214v1